Received: 18 September 2018 | Revised: 22 April 2019 | Accepted: 21 May 2019 | Published on: 13 June 2019

DOI: 10.1002/joc.6170

RESEARCH ARTICLE

International Journal of Climatology RMetS

Multi-model analysis of climate impacts on plant photosynthesis in China during 2000–2015

Hao Yan[1,8] | Shao-Qiang Wang[2] | Jun-Bang Wang[2] | Yun Cao[1] | Ling-Ling Xu[1] | Men-Xin Wu[1] | Lu Cheng[1] | Liu-Xi Mao[1] | Feng-Hua Zhao[2] | Xian-Zhou Zhang[2] | Yun-Fen Liu[2] | Yan-Fen Wang[3] | Shi-Ping Chen[3] | Ying-Nian Li[4] | Shi-Jie Han[5] | Guo-Yi Zhou[6] | Yi-Ping Zhang[7] | Herman H. Shugart[8]

[1]National Meteorological Center, China Meteorological Administration, Beijing, China

[2]Key Laboratory of Ecosystem Network Observation and Modeling, Institute of Geographic Sciences and Natural Resources Research, Chinese Academy of Sciences, Beijing, China

[3]Institute of Botany, Chinese Academy of Sciences, Bejing, China

[4]Northwest Institute of Plateau Biology, Chinese Academy of Sciences, Xining, China

[5]Institute of Applied Ecology, Chinese Academy of Sciences, Shenyang, China

[6]South China Botanical Garden, Chinese Academy of Sciences, Guangzhou, China

[7]Xishuangbanna Tropical Botanical Garden, Chinese Academy of Sciences, Yunnan, China

[8]Environmental Sciences Department, University of Virginia, Charlottesville, Virginia

Correspondence

Hao Yan, National Meteorological Center, China Meteorological Administration, Beijing 100081, China.
Email: yanhaon@hotmail.com

Funding information

National Aeronautics and Space Administration; National Natural Science Foundation of China, Grant/Award Number: 41571327, 31700421; National Key Research and Development Program of China, Grant/Award Number: 2017YFC0503803; Oak Ridge National Laboratory; Seoul National University; University of Montana; United States Geological Survey; Chinese Academy of Sciences; National Bureau of Statistics of China

Abstract

Differences, arising from differences in gross primary production (GPP) model structures and driving forces, have fuelled arguments concerning interannual changes of GPP in China since 2000. To better investigate the interannual variability of GPP and its covariance with climate factors in China, this study adopted a multi-model analysis based on three GPP models (i.e., Terrestrial Ecosystem Carbon flux model [TEC], Breathing Earth System Simulator model [BESS], and MOD17 GPP model). The results show that annual GPP in China increased by 0.021–0.057 Pg C year^{-1} from 2000 to 2015 attributable to atmospheric-CO_2 fertilization effects and favourable climate change, that is, increasing precipitation (P_r) and temperature (T_a). However, northern China and southern China had a large difference in the amplitude of these GPP changes; annual GPP increased by 0.017–0.039 Pg C year^{-1} in northern China but only 0.001–0.018 Pg C year^{-1} in southern China. Northern China and southern China occupy contrasting climate zones and this contrast produced different interannual variability of GPP through different mechanisms. Northern China has a dry climate with GPP changes sensitive to P_r. As a result, more P_r along with higher T_a in northern China produced the strong uptrend of GPP from 2000 to 2015. In contrast, southern China has a wet climate with its GPP sensitive to solar radiation and T_a. For the interval of 2000–2015, decreasing radiation plus drought exerted a negative influence on GPP in southern China. This study highlights the diverse mechanisms in which climate change affects GPP in dry and wet climate zones. A robust multi-model analysis is preferred to reduce uncertainties arising from a single GPP model and its driving data.

KEYWORDS

climate change, dry/wet climate, Gross primary production, meteorological factors, multi-model analysis

1 | INTRODUCTION

Atmosphere carbon dioxide (CO_2) concentration has steadily increased from 277 ppmv in 1850, regarded as the beginning of the industrial era, to 400 ppmv in 2016 (Dlugokencky and Tans, 2017). Anthropogenic emissions from fossil fuels and industry have been the dominant source of the atmosphere CO_2 increase since 1920 (Le Quéré *et al.,* 2016). Cumulative emissions of CO_2 result in the global temperature rising, that is, long-term anthropogenic warming (Millar *et al.,* 2017). Numerous studies (Cao *et al.,* 2002, 2005; Nemani *et al.,* 2003; Los, 2013; Schimel *et al.,* 2015; Zhu *et al.*, 2016, 2016) have found that the atmospheric CO_2 increase in conjunction with climate change enhances plant photosynthesis, which in turn removes CO_2 from atmosphere and produces more organic matter, for example, gross primary production (GPP). This forms a feedback mechanism between plants and environment. Ground-based evidence from Chinese forest inventories also shows that global environmental changes stimulate forest growth and thus enhance forest C sequestration (Fang *et al.,* 2014).

China has released a large amount of industrial and energy-related CO_2 since 2000 (Grubb *et al.,* 2015; Jiang and Ryu, 2016), and simultaneously has carried out numerous afforestation projects under national conservation policies (Yuan *et al.,* 2014, 2014b; Ouyang *et al.,* 2016). Thus, the issue of degree to which China's carbon sequestration through plant photosynthesis offsets China's carbon emissions is significant.

However, predicted interannual variations of GPP in China produced by different GPP models driven with different satellite-based vegetation products and climate data have produced conflicting results (Li *et al.,* 2013; Liu *et al.,* 2013; Wang *et al.,* 2017, 2017; Yao *et al.,* 2018). Arising from different model structures as well as satellite and meteorological driving data (Li *et al.,* 2013; Liu *et al.,* 2013), some of these report decreasing GPP trends in China. Thus, multi-model analyses are needed to investigate interannual variations of GPP in China. This is the first objective of this study.

Various vegetation types, which are geographically associated with distinct climate zones, cover China. Arid and semiarid climate zones in northern China often have sparse vegetation types such as desert and grassland due to scarce precipitation (Figure 1). However, southern China, which occupies a humid-subtropical-climate zone with ample precipitation and warmth, has dense vegetation types such as evergreen forests (Yao *et al.,* 2018). Because vegetation is subject to different climate factors in northern and southern China, it is not clear whether vegetation had an identical responses to climate change in these two regions over 2000–2015. This determination is the second objective of this study.

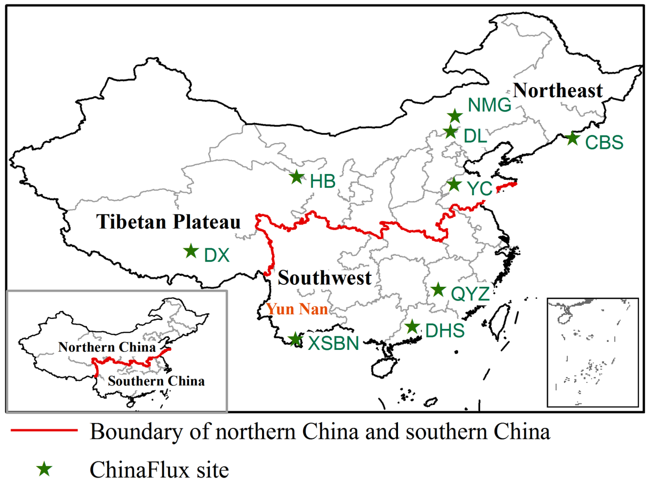

FIGURE 1 Distribution of nine ChinaFlux site, Tibetan plateau, southwest region, northeast region, and Yun Nan province in China. The black line shows the boundary of northern China and southern China [Colour figure can be viewed at wileyonlinelibrary.com]

Earth observation (EO) products have supported global ecology applications Pfeifer *et al.,* 2012). They are a basis for GPP estimates and test/constrain large-area GPP models. Many GPP studies over China were based on early Terra MODIS C5 vegetation products (Li *et al.,* 2013; Liu *et al.,* 2013; Wang *et al.,* 2017, 2017). Zhang *et al.* (2017) pointed out that Terra MODIS C6 vegetation index (VI) product has a substantial differences in global vegetation trends relative to previous Terra MODIS C5 VI products. This arises from an improved calibration approach (Lyapustin *et al.,* 2014). Much of the "browning" trends in vegetation detected by MODIS Terra-C5 VI may have resulted from the sensor degradation (Wang *et al.,* 2012; Zhang *et al.,* 2017). Hence, it is important to quantify the impact of Terra MODIS C5 and C6 vegetation products on GPP trends, the third objective of this study.

Our study analyzes spatial-temporal patterns of GPP in China, northern China, and southern China since 2000 based on a multi-model analysis from three GPP models. The elements of our study, presented in sections below, are:

1. An evaluation of the TEC GPP model (Yan *et al.,* 2015), the Breathing Earth System Simulator (BESS) and the MOD17 GPP products against observed GPP at nine flux tower sites in China;
2. A multi-model analysis of interannual changes of GPP in response to climate change in China, northern China, and southern China since 2000;
3. A diagnostic analysis of MODIS C5 and C6 FPAR products and their impacts on simulated TEC GPP trends.

Two of these three models, the BESS and the MOD17 GPP models, have been evaluated at flux tower sites in China (Jiang and Ryu, 2016; Zhu *et al.,* 2016, 2016). The other, the TEC GPP model, has been evaluated primarily at AmeriFlux sites (Yan *et al.,* 2015).

2 | DATASETS AND PROCESSING PROCEDURE

2.1 | Meteorological data

Monthly meteorological data at 2000 high-density stations across China for the period of 2000–2015 were obtained from the National Meteorological Information Center (NMIC; http://data.cma.cn) of Chinese Meteorological Administration (CMA). Meteorological variables include air temperature, water vapour pressure, air relative humidity, precipitation, wind speed, and hours of sunshine. Station data, continuously recorded over the research period, were quality checked by National Meteorological Information Centre according to the meteorological standard (QX/T 118–2010) for quality control of surface meteorological observational data (see: National Meteorological Information Center, 2010).

To drive the TEC-GPP model, meteorological station data were interpolated to a spatial resolution of $0.08^\circ \times 0.08^\circ$ latitude/longitude by using an Inverse Distance Weighted (IDW) interpolation method. Monthly incident global radiation (Q) and net radiation (R_n) were calculated from sunshine hour according to the Food and Agriculture Organization (FAO) method (Allen *et al.,* 1998). The FAO R_n method has been evaluated against observations at the Qianyanzhou flux tower site in southern China and then further applied to drought research in China (Yan *et al.,* 2016, 2016b).

2.2 | MOD15A2 LAI/FPAR products

The Moderate Resolution Imaging Spectroradiometer (MODIS) is a key instrument onboard the National Aeronautics and Space Administration (NASA) sun-synchronous Terra satellite (10:30 a.m. local time descending node) and Aqua satellite (1:30 p.m. local time ascending node). MODIS LAI/FPAR products (MOD15A2) from the Terra satellite were downloaded (https://e4ftl01.cr.usgs.gov/MOLT/), and applied as drivers for the TEC GPP model. This quantified the impact of Collections 6 (C6) and 5 (C5) MOD15A2 data on simulated TEC GPP trend in China. The latest C6 MOD15A2H data with improved calibration has a spatial resolution of 500 m while the C5 MOD15A2 data operates at 1 km spatial resolution.

The MODIS LAI/FPAR products were derived from up to seven MODIS spectral bands using a three-dimensional-radiative transfer model for a vegetation canopy (Myneni *et al.,* 2002). If the main radiative transfer algorithm failed due to clouds or other atmospheric conditions (Yang *et al.,* 2006), a back-up LAI/FPAR algorithm (based on empirical MODIS-specific NDVI-LAI and NDVI-FPAR relationships) was used. LAI/FPAR data also were checked for quality control in this study. MOD15A2 LAI/FPAR products supply quality control data (i.e., FparLai_QC) accompanied with LAI/FPAR data. If a pixel was cloudy as shown by FparLai_QC, it was replaced by linear interpolation from the nearest reliable data as appropriate.

2.3 | Land cover and soil data

Land cover data with a classification system that included evergreen coniferous forest, deciduous coniferous forest, evergreen broadleaf forest, deciduous broadleaf forest, mixed forest, shrub, grassland, cropland, wetland, city, water body, desert, ice and snow at a 1 km spatial resolution was selected from National Resources and Environments Database of China (http://www.resdc.cn/data.aspx?DATAID=97) for the year 2000. The land cover classification was derived from Landsat Thematic Mapper (TM) digital images collected in 1999/2000 using a human-machine interactive interpretation method to increase classification consistency and accuracy (Liu *et al.,* 2002, 2003).

Soil data in China at a 5×5 arc-minute (i.e., 0.08°) resolution was from the Global Gridded Surfaces of Selected Soil Characteristics developed by the International Geosphere-Biosphere Programme (IGBP) Data and Information Services (DIS). The data set contains profile available water capacity (PAWC), field capacity, wilting point, soil-carbon density, total nitrogen density, thermal capacity, and bulk density for a soil depth of 0–150 cm (Global Soil Data Task Group, 2000).

2.4 | Forest resource and inventory data in China

Annual afforestation area since 2000 was downloaded from the National Bureau of Statistics of China at a website of http://www.stats.gov.cn. National forest inventories have been periodically implemented to document the forest information about area, timber volume, age, and type. Forest area data used in this study covers the two periods of 1999–2003 and 2009–2013 (Chinese Ministry of Forestry, 2004, 2014).

2.5 | Eddy covariance data from ChinaFLUX

The eddy covariance (EC) method measures CO_2, water, and energy fluxes between biosphere and the atmosphere. EC observations at flux tower sites have been adopted to evaluate both light use efficiency (LUE) and process-based GPP models (Baldocchi *et al.,* 2001). The EC method directly measures net ecosystem exchange (NEE) not GPP. GPP is calculated as the difference between measured daytime NEE and daytime respiration estimated from a temperature-dependent model (Falge *et al.,* 2001, 2002). Therefore, the GPP estimates include all uncertainties of the NEE measurement and of the daytime respiration model.

In this study, EC data, observed at nine Chinese Terrestrial Ecosystem Flux Research Network (ChinaFLUX) tower sites (Figure 1) covering various biome types such as forest, grasslands, and cropland (Table 1), all spanned three continuous years and were adopted to evaluate the TEC GPP model. As a long-term national network of micrometeorological flux measurement sites, ChinaFLUX is designed to explore the dynamics and underlying mechanisms of carbon and water exchange and to quantify the biotic and abiotic effects on ecosystem processes (Yu *et al.,* 2013; Huang *et al.,* 2014; Wang *et al.,* 2015).

2.6 | Data pre-processing

All model forcing data including MODIS C6 and C5 LAI/FPAR data, meteorological data, land cover data, and PAWC of soil data, were interpolated to a 0.08° × 0.08° grid resolution and then applied to driving the TEC GPP model on a monthly timescale. The TEC GPP_{C6} and GPP_{C5} products were used in the multi-model analysis combined with available BESS GPP_{C5} and MOD17A3 GPP_{C5} products. Linear regression was adopted in this study to analyse inter-annual trends of GPP products and model forcing data over 2000–2015.

2.7 | BESS GPP products

The BESS, a simplified process-based model, simulates atmosphere and canopy radiative transfers, canopy photosynthesis, transpiration, and energy balance (Ryu *et al.,* 2011). The monthly BESS GPP products at 0.5°geographic resolution for a period of 2000–2015 were downloaded (http://environment.snu.ac.kr/bess_flux/) in this study. The BESS GPP and ET products were calculated from:

1. MCD15A2 C5 LAI products composited from Terra C5 MOD15A2 and Aqua C5 MYD15A2 products,
2. MODIS atmosphere C6 products, four other satellite datasets, and
3. Four reanalysis datasets.

The BESS products have been comprehensively evaluated against FLUXNET 2015 dataset including China flux tower data and MPI-BGC and official MODIS products at multiple spatial and temporal scales (Jiang and Ryu, 2016).

2.8 | MOD17 GPP products

The MOD17A3 C55 annual GPP products at 1 km spatial resolution and MOD17A2 C55 monthly GPP products at 5 km spatial resolution were downloaded from the Numerical Terradynamic Simulation Group (NTSG, http://www.ntsg.umt.edu/project/mod17) for comparison with GPP trend estimates from the TEC GPP model in this study. The MODIS GPP algorithm (Running *et al.,* 2004) follows the Monteith LUE theory (1972),

$$\mathrm{GPP} = \varepsilon^* \times m(T_{\min}) \times m(\mathrm{VPD}) \times \mathrm{FPAR} \times \mathrm{PAR} \quad (1)$$

where ε^* is the biome-specific maximum conversion efficiency, $m(T_{\min})$ reduces $\varepsilon_{\max}$ as a scaler when the minimum air temperature ($T_{\min}$) limits plant growth, VPD is vapour pressure deficit, and m (VPD) is another scaler used to

TABLE 1 Site name, abbreviation (Abbr), latitude (lat), longitude (long), altitude (alt), climate, biome type, and years of data of nine ChinaFlux sites

Site name	Abbr	Lat/long	Alt (m)	Climate	Biome type	Years
ChangBaiShan	CBS	41.40/128.09	738	Temperate	Mixed forest	2003–2005
QianYanZhou	QYZ	26.74/115.06	100	Subtropical	Evergreen needleleaf forest	2003–2005
DingHuShan	DHS	23.17/112.53	300	Subtropical	Evergreen broadleaf forest	2003–2005
XiShuangBanNa	XSBN	21.95/101.20	750	Tropical	Seasonalrain forest	2004–2006
NeiMengGu	NMG	43.54/116.67	1,200	Temperate	Grassland	2003–2005
DangXiong	DX	30.49/91.06	4,300	Alpine	Grassland	2004–2006
HaiBei	HB	37.66/101.33	3,202	Alpine	Grassland	2003–2005
DuoLun	DL	42.04/116.28	1,350	Temperate	Grassland	2010–2012
YuCheng	YC	36.95/116.60	28	Temperate	Cropland	2003–2005

reduce ε^* when VPD is high enough to inhibit photosynthesis, PAR is the incident photosynthetically active radiation, and FPAR is the fraction of PAR absorbed by the canopy.

The MOD17 global GPP products were calculated from MOD15A2 Collection 5 FPAR/LAI products, biome type-specific maximum conversion efficiency, and the National Centers for Environmental Prediction (NCEP) and the National Center for Atmospheric Research (NCAR) Reanalysis II data (Zhao and Running, 2010). MOD17 GPP products have been used in studying the drought impact in China (Zhang *et al.,* 2012) and the MOD17 GPP model has been evaluated using China flux tower data (Zhu et al., 2016, 2016).

3 | DESCRIPTION OF THE TEC GPP MODEL

The TEC model (Yan *et al.,* 2015) simulates GPP of terrestrial ecosystem from the LUE model (Equation (1)) suggested by Monteith (1972). As the LUE ε varies with several environmental and vegetation-related parameters (Maisongrande *et al.,* 1995; Ruimy *et al.,* 1999; Garbulsky *et al.,* 2010), temperature and water stresses are taken into consideration in TEC-GPP model,

$$\mathrm{GPP} = \varepsilon \times \mathrm{FPAR} \times \mathrm{PAR} \tag{2}$$

$$\varepsilon = \varepsilon^* \times T_\varepsilon \times W_\varepsilon \tag{3}$$

where ε^* is the maximum light use efficiency, PAR is the incident photosynthetically active radiation (MJ m^{-2} month^{-1}), and T_ε and W_ε account for effects of temperature stress and water stress on LUE of ecosystem, respectively. PAR is assumed to be a 0.48 fraction of the incident global radiation Q (McCree, 1972). TEC uses a universal ε^* with a value of 1.8 gC MJ^{-1} from field observations for C_3 species (Waring *et al.,* 1995; Landsberg and Waring, 1997). As leaf photosynthetic rates of C_4 species are greater than those of C_3 species (Baldocchi, 1994; Prince and Goward, 1995), TEC uses a universal $\varepsilon^* = 2.76$ g C MJ^{-1} for C_4 species as suggested by Prince and Goward (1995). T_ε is calculated using the temperature stress equation developed for the Terrestrial Ecosystem Model (Raich *et al.,* 1991).

The water stress factor W_ε in the TEC GPP model is defined as,

$$W_\varepsilon = \frac{E}{E_{\mathrm{PT}}} \tag{4}$$

where E is actual evapotranspiration calculated from the ARTS E Model (Yan *et al.,* 2012), and E_{PT} is the Priestley and Taylor (1972) model for potential evaporation.

4 | DEFINITION OF THE METEOROLOGICAL COMPREHENSIVE FACTOR AND THE HUMIDITY INDEX

To analyse the total impact of meteorological factors on GPP, a meteorological comprehensive factor (M_c) was calculated,

$$M_c = \mathrm{PAR} \times T_\varepsilon \times W_\varepsilon \tag{5}$$

To investigate the spatial relationship between arid/wet conditions and mean annual GPP, annual humidity index (H_i) was calculated from annual precipitation divided by annual potential evapotranspiration,

$$H_i = \frac{\sum P_r}{\sum E_{P\_\mathrm{Allen}}} \tag{6}$$

$$E_{P\_\mathrm{Allen}} \frac{0.408\Delta(R_n - G) + \gamma \frac{900}{T+273} u\mathrm{VPD}}{\Delta + \gamma(1 + 0.34u)} \tag{7}$$

where E_{P_Allen} is potential evapotranspiration (Allen *et al.,* 1998), R_n is net radiation (MJ m^{-2} day^{-1}), T_a is the air temperature (°C), Δ is the gradient of the saturated vapour pressure to the air temperature (kPa), γ is the psychrometric constant, VPD is the vapour pressure deficit, u is the wind speed (m s^{-1}) at 2 m height.

5 | RESULTS

5.1 | Evaluation of estimated TEC GPP against observed GPP at flux tower sites on monthly scales

Figure 2 shows that TEC $\mathrm{GPP}_{\mathrm{C6}}$ simulated seasonal variations of GPP observed at nine flux tower sites of ChinaFLUX in China. The GPP statistics (Table 2) vary by flux site and ecosystem type with R^2 between 0.51 at DHS site and 0.95 at NMG site. The RMSE similarly ranges from 14.6 g C m^{-2} mo^{-1} at NMG to 137.0 g C m^{-2} mo^{-1} at YC, and the Bias is between −82.3 g C m^{-2} mo^{-1} at YC and 26.5 g C m^{-2} mo^{-1} at XSBN. TEC $\mathrm{GPP}_{\mathrm{C6}}$ products underestimated GPP at two sites of DHS (RMSE = 56.3 g C m^{-2} mo^{-1}, Bias = −29.1 g C m^{-2} mo^{-1}, and R^2 = 0.51) and YC (RMSE = 137.0 g C m^{-2} mo^{-1}, Bias = −82.3 g C m^{-2} mo^{-1}, and R^2 = 0.65).

TEC $\mathrm{GPP}_{\mathrm{C6}}$ underestimated GPP in winter at the subtropical forest site of DHS (Figure 2(c)). The DHS flux tower site, is located in mountainous areas with a large landscape heterogeneity, and may not be well represented by the remote sensing FPAR data and interpolated-meteorological data on the 8 km scale. Similarly, the TL-LUE GPP model

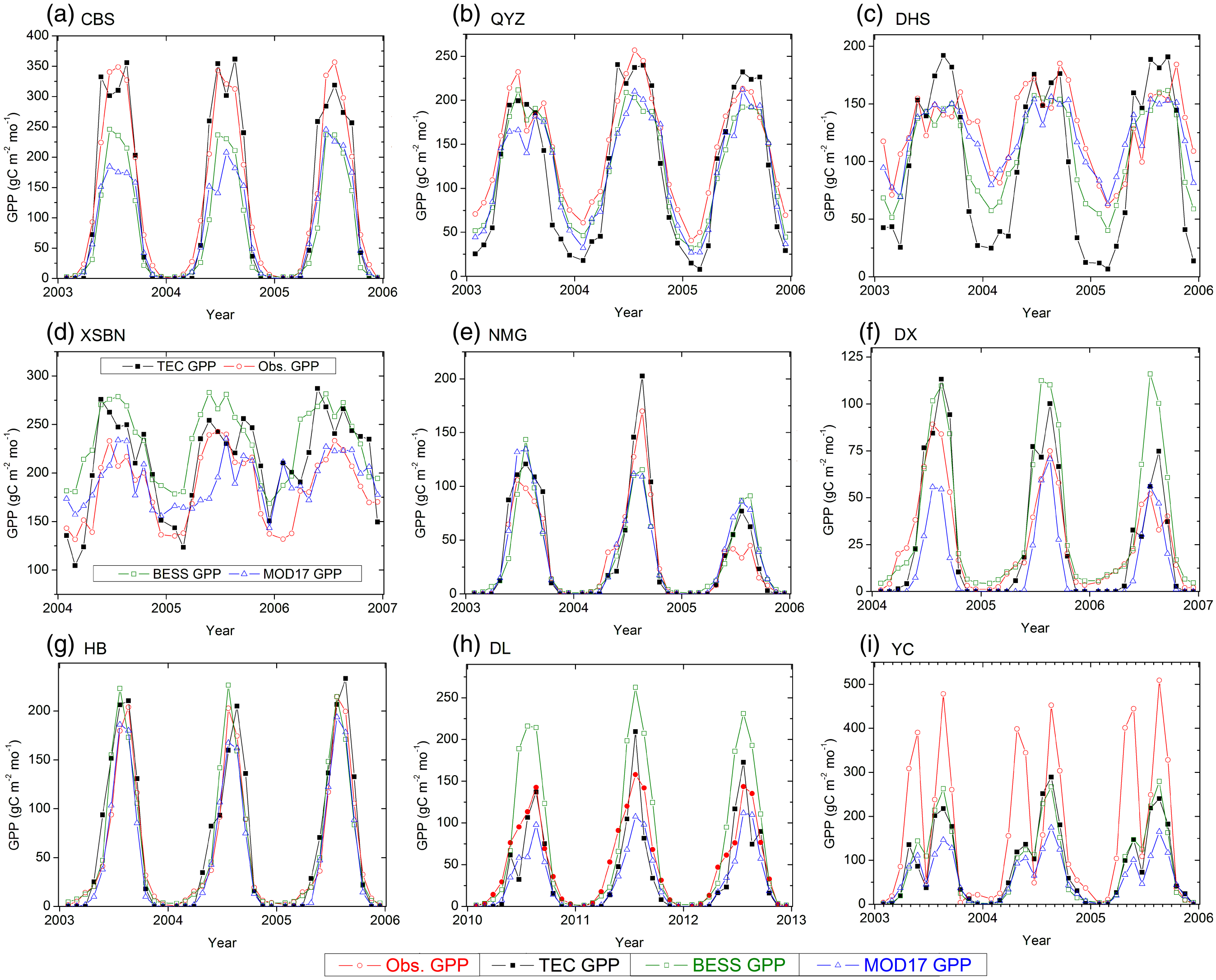

FIGURE 2 Seasonal variations of monthly estimated TEC GPP_{C6}, BESS GPP_{C5}, and MOD17A2 GPP_{C5}, and flux tower-observed GPP at nine flux tower sites, that is, (a) CBS, (b) QYZ, (c) DHS, (d) XSBN, (e) NMG, (f) DX, (g) HB, (h) DL, and (i) YC [Colour figure can be viewed at wileyonlinelibrary.com]

TABLE 2 Statistics of estimated monthly TEC GPP_{C6}, BESS GPP_{C5}, and MOD17 GPP_{C5} versus flux tower observed GPP at nine ChinaFlux sites

Site Name	TEC			BESS			MOD17		
	R^2	RMSE	Bias	R^2	RMSE	Bias	R^2	RMSE	Bias
CBS	0.92	39.7	−2.3	0.97	65.6	−50.2	0.92	74.4	−48.8
QYZ	0.91	38.8	−24.1	0.94	25.2	−20.5	0.93	29.0	−24.0
DHS	0.51	56.3	−29.1	0.61	31.6	−20.0	0.72	19.3	−7.6
XSBN	0.64	39.0	26.5	0.79	50.0	46.9	0.43	27.8	6.1
NMG	0.95	14.6	4.4	0.78	20.3	0.7	0.81	19.4	2.3
DX	0.85	15.7	1.3	0.83	22.1	11.3	0.78	17.2	−12.3
HB	0.92	23.1	6.9	0.93	18.9	3.0	0.97	14.0	−8.3
DL	0.79	27.4	−12.1	0.9	47.0	22.9	0.94	47.0	−20.7
YC	0.65	137.0	−82.3	0.65	135.7	−81.6	0.78	164.9	−109.7

Percent of variance explained (R^2), root-mean-square-error (RMSE), and bias (g C m^{-2} mo^{-1}).

(He *et al.,* 2013) reported a similarly poor statistics of R^2 = 0.48 and RMSE = 39.9 g C m^{-2} mo^{-1} at DHS. The YC site, a two-season-rotation-crop site that is planted with winter wheat and summer maize, had an underestimated TEC GPP in growing season. The MODIS LAI/FPAR products are underestimated for crop (Verma *et al.,* 2005), and field measurements shows that the YC site has a higher value of LAI of as much as 6.5 (Wang *et al.,* 2007).

Figure 3(a) indicates that TEC GPP_{C6} had overall statistics of R^2 = 0.71, Bias = −12.3 g C m^{-2} mo^{-1}, and RMSE = 56.1 g C m^{-2} mo^{-1} for all data (*N* = 324) from 9 flux tower sites on a monthly scale in comparison with flux tower-observed GPP. TEC GPP_{C6} had an underestimated GPP of −11.8%, mainly caused by the underestimation at the YC crop site. Excluding the YC site, TEC GPP_{C6} produced an improved performance with R^2 = 0.87, Bias = −3.5 g C m^{-2} mo^{-1} (−3.7%), and RMSE = 34.5 g C m^{-2} mo^{-1} for C3 vegetation types (*N* = 288) from 8 flux tower sites. Similarly, EC-LUE GPP model had statistics of R^2 = 0.79 and R^2 = 0.62 for C3 vegetation and C4 crop types, respectively (Li *et al.,* 2013).

5.2 | Evaluation of the BESS and MOD17 GPP products against observed GPP at flux tower sites on monthly scales

The seasonal variations in output from the BESS and MOD17 GPP models simulated for nine flux tower sites of ChinaFLUX in China showed good qualitative agreement (Figure 2). When quantitatively compared with flux tower-observed GPP for these nine flux tower sites (Figure 3(b)), BESS GPP_{C5} had a monthly statistics of R^2 = 0.68, Bias = −9.7 g C m^{-2} mo^{-1}, and RMSE = 58.0 g C m^{-2} mo^{-1} for all data (*N* = 324). However, MOD17 GPP_{C5} had a similar R^2 = 0.67, but Bias = −24.8 g C m^{-2} mo^{-1} and RMSE = 63.5 g C m^{-2} mo^{-1} for all data (Figure 3(c)). MOD17 GPP_{C5} underestimated GPP by 23.8% on average.

Further evaluation (Table 2) shows that MOD17 GPP_{C5} underestimated GPP at seven sites. The Bias of MOD17 GPP ranges from −109.7 g C m^{-2} mo^{-1} at YC to 6.1 g C m^{-2} mo^{-1} at XSBN, and the RMSE changes from 14.0 g C m^{-2} mo^{-1} at HB to 164.9 g C m^{-2} mo^{-1} at YC. For BESS GPP, the Bias is between −81.6 g C m^{-2} mo^{-1} at YC and 46.9 g C m^{-2} mo^{-1} at XSBN, and the RMSE ranges from 18.9 g C m^{-2} mo^{-1} at HB to 135.7 g C m^{-2} mo^{-1} at YC.

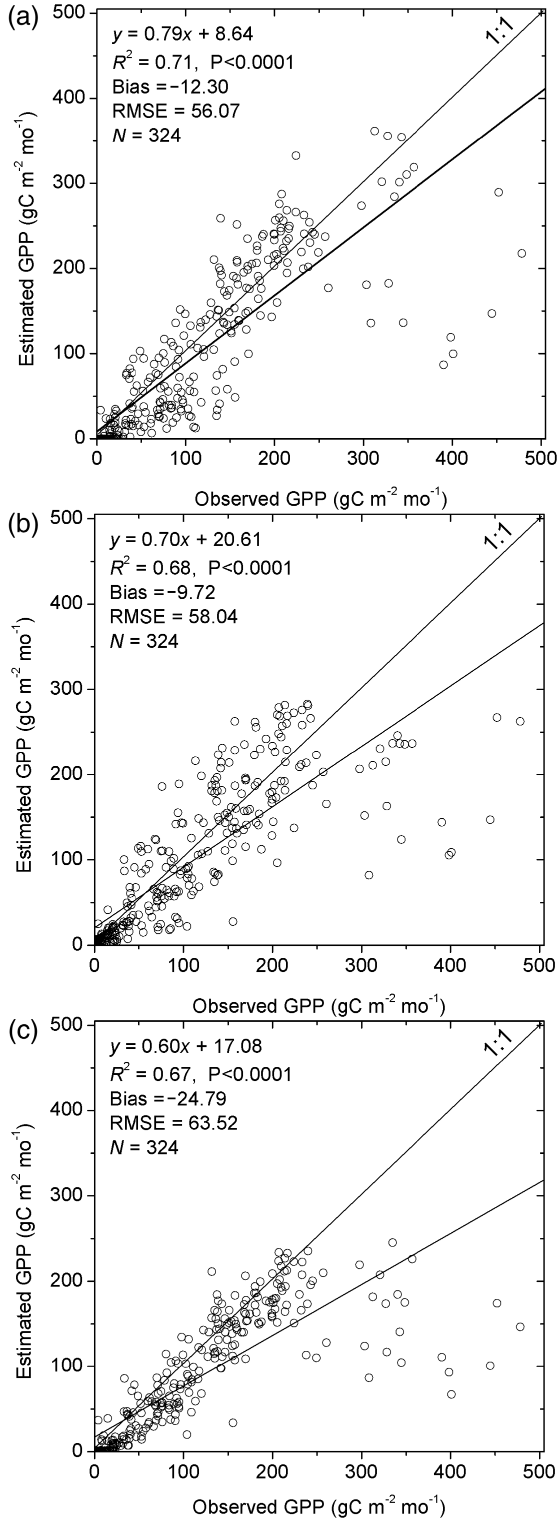

FIGURE 3 Comparison of the flux tower-observed GPP versus estimated (a) TEC GPP_{C6}, (b) BESS GPP_{C5}, and (c) MOD17A2 GPP_{C5} for all data from 9 flux tower sites on a monthly scale

5.3 | Spatial characteristic of mean annual GPP and humidity index in China

The mean annual GPP from the three GPP models all had a large spatial heterogeneity (Figure 4). Overall, GPP decreased from south to north and from east to west. In southeastern China, GPP had the highest value of over 2,500 gC m^{-2} $year^{-1}$ while in western China, GPP had the lowest value below 50 gC m^{-2} $year^{-1}$. TEC GPP_{C6}, BESS GPP_{C5}, and MOD17A3 GPP_{C5} products had an average annual GPP of 7.03 Pg C year^{-1}, 6.42 Pg C year^{-1}, and 5.97 Pg C year^{-1} for 2000–2015 within the reported GPP ranges of 5.58 ± 1.92 Pg C year^{-1} for China derived from multiple LUE models and process-based GPP models (Li *et al.,* 2013).

This spatial pattern of annual GPP was subject to climate factors including light, temperature, and precipitation. Figure 5(a) shows the pattern of GPP agreed well with spatial pattern of mean annual humidity index (H_i) for the same period of 2000–2015. Note that annual H_i was defined as annual precipitation divided by annual E_{P_Allen}. Most of southern China featured a humid climate with a higher H_i up to 1.3–1.8 and a higher GPP above 1,500 gC m^{-2} year^{-1}. However, northern China's dryer climate had a lower H_i down to 0.1–0.5 and a lower GPP below 700 gC m^{-2} year^{-1}, which means that annual precipitation could not satisfy the evaporation demand. One would expect plant growth in northern China to be stressed by water deficit and for GPP to be dominated by the precipitation factor.

Further correlation analysis of TEC GPP $_{C6}$ against meteorological factors on yearly scales (Figure 5(b); Table 4) revealed that GPP in the northern China was primarily controlled by precipitation. GPP in humid southern China was dominated by temperature and radiation factors, which suggests that interannual changes of GPP in northern China and southern China were driven by contrasting mechanisms in their responses to climate change over 2000–2015. These findings match those of Yuan et al. (2014, 2014) and Zhang *et al*. (2018), who pointed out that water availability is the most important factor controlling GPP changes over northern China and Tibetan Plateau. GPP in southern China is

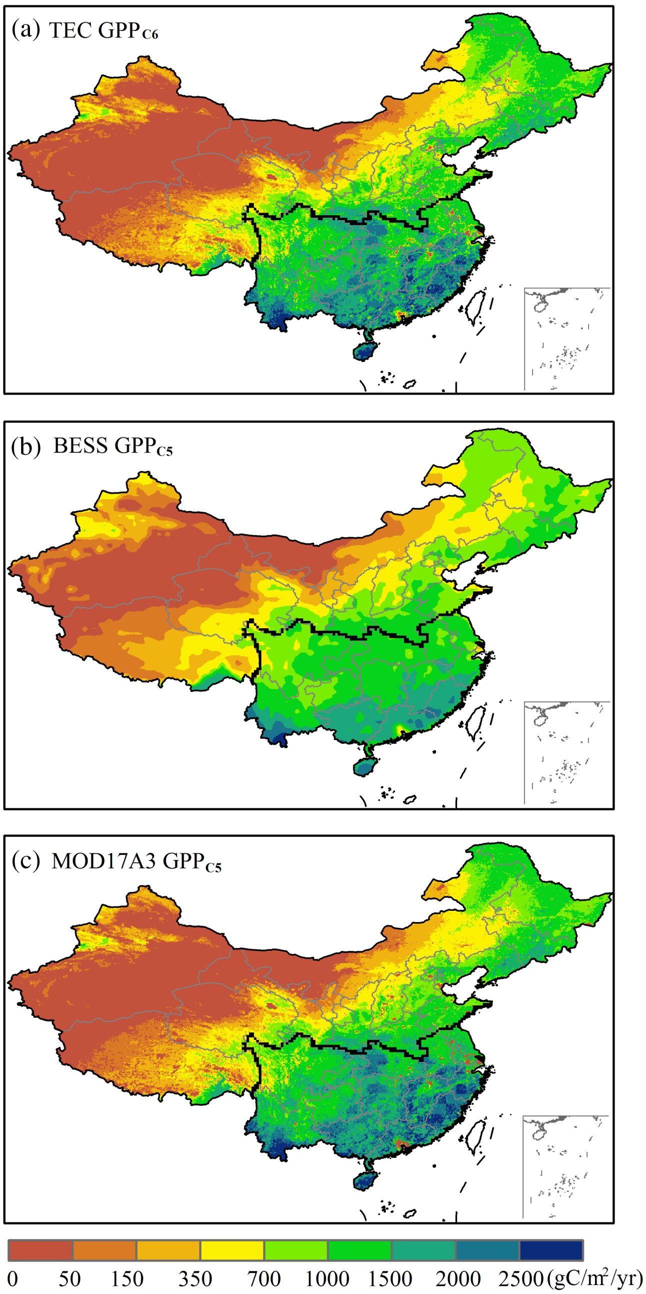

FIGURE 4 Mean annual (a) TEC GPP$_{C6}$, (b) BESS GPP$_{C5}$, and (c) MOD17A3 GPP$_{C5}$ over 2000–2015 in China [Colour figure can be viewed at wileyonlinelibrary.com]

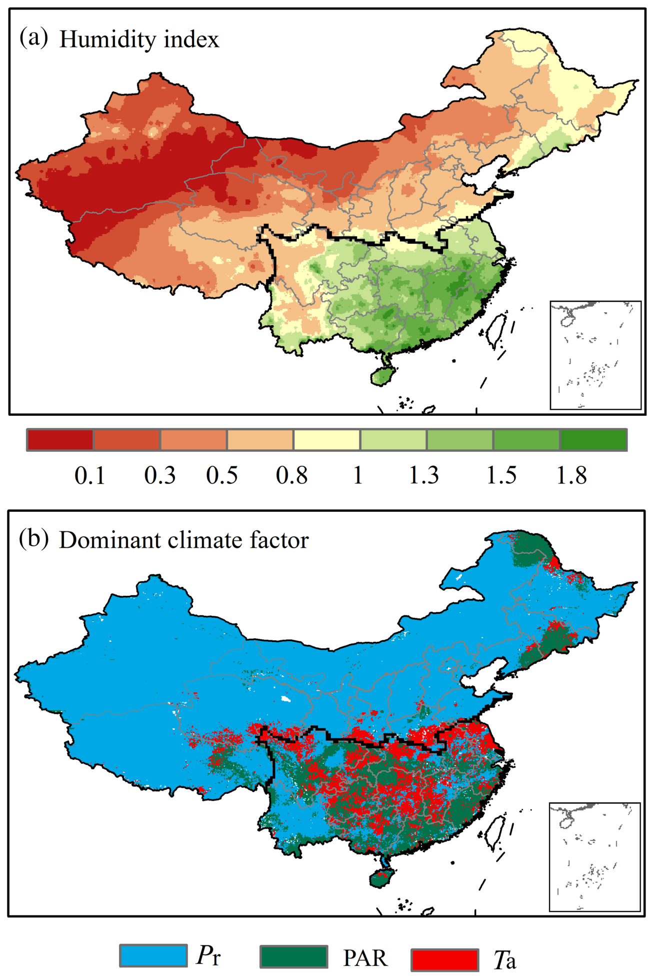

FIGURE 5 (a) Mean annual humidity index and (b) dominant climate factor of GPP interannual variability across China over 2000–2015 [Colour figure can be viewed at wileyonlinelibrary.com]

dominated by temperature and radiation factors (Yao *et al.,* 2018).

5.4 | Multi-model analysis of interannual changes of GPP in China, northern and southern China since 2000

Figure 6(a) shows that all four GPP products from three GPP models had an increasing trend ($p < 0.05$) from 2000 to 2015 with different amplitudes. TEC GPP_{C6} had the highest growth rate of 0.057 Pg C $year^{-1}$, which was double that of the increasing amplitude of the other three GPP products. Driven with the same MODIS C5 LAI/FPAR products, TEC GPP_{C5} tended to increase at a rate of 0.033 Pg C $year^{-1}$ over 2000–2015 comparable to increasing rates of 0.037 and 0.021 Pg C $year^{-1}$ for BESS and MOD17A3, respectively, which shows that TEC, BESS, and MOD17A3 products had similar potential in revealing interannual variations of GPP in China. Note that BESS GPP_{C5} products started from 2001. Table 3 shows that four GPP products for entire China increased by 5–13% from 2000 to 2015.

For northern China (Figure 6(c)), annual GPP of all four products had an increasing trend ($p < 0.01$) from 2000 to 2015. However, in southern China (Figure 6(e)), only TEC GPP_{C6} and BESS GPP_{C5} showed an increasing trend ($p < 0.05$). TEC GPP_{C5} and MOD17A3 GPP_{C5} had an insignificant increasing trend. Northern China had a higher increasing amplitude of annual GPP than that of southern China. Comparisons (Table 3) showed that the annual GPP of the four GPP products increased by 10–22% for northern China and only 0–6% for southern China over 2000–2015.

The spatial pattern of linear trends (Figure 6(b), (d), (f), (g)) shows annual GPP with significant increases ($p < 0.05$), primarily in northern China for the four GPP products. Most of southern China had no significant GPP changes ($p > 0.05$). A large difference also existed in spatial distribution of changing amplitude for four GPP model products. TEC GPP_{C6} (Figure 6(b)) had a larger area with linear trends of absolute $k > 25$ g C $year^{-1}$ m^{-2}, while TEC GPP_{C5} (Figure 6(d)) had more areas of decreasing trend with $k < 0$ g C $year^{-1}$ m^{-2} in southern China consistent with the decreasing trend of $FPAR_{C5}$ (Figure 4(c)). BESS (Figure 6(f)) and MOD17A3 (Figure 6(g)) GPP_{C5} often had a linear trend with absolute $k < 25$ g C $year^{-1}$ m^{-2} across China.

5.5 | Interannual changes of meteorological factors in China, northern and southern China since 2000

Figure 7 shows interannual variations of PAR, T_a, P_r, and their comprehensive factor (M_c) from 2000 to 2015 in China. Figure 7(a) and (b) indicates annual PAR decreased ($p > 0.17$) for China, northern China and southern China. Northern China's spatial pattern of interannual changes (Figure 7(c)) has a decreasing trend in PAR ($k < -10$ MJ m^{-2} $year^{-1}$). The Southwest region had an increasing trend in PAR ($k > 10$ MJ m^{-2} $year^{-1}$).

Mean annual T_a increased ($p > 0.25$; Figure 7(d), (e)) from 2000 to 2015 in China, northern China and southern China. Figure 7(f) shows that T_a had an increase ($k > 0.025°$C $year^{-1}$) mainly in Tibetan Plateau and Southwest region. Other Chinese regions had no significant trend in T_a.

Annual P_r increased ($p > 0.22$; Figure 7(g), (h)) from 2000 to 2015 in China, northern China and southern China. Figure 7(i) indicates annual P_r increased in Northeast China and decreased mainly in the Southwest region. Other Chinese regions had no significant trend in P_r.

Annual M_c increased ($p = 0.26$; Figure 7(j)) from 2000 to 2015 in China. However, northern China and southern China had contrasting trends in M_c from 2000 to 2015. Figure 7(k) shows that annual M_c in northern China tended to increase while southern China had a decrease in annual M_c. Figure 7(i) indicates that a primary increase of M_c mainly distributed in northern China and a decrease mainly located in Southwest region of China.

Increasing annual P_r and T_a produced the significant increase in M_c for northern China, which had favoured plant growth since 2000. However, decreasing annual PAR produced the decrease in M_c for southern China, that is, meteorological conditions disadvantaged plant growth from 2000 to 2015. As a result, GPP in northern China increased ($p < 0.01$) by 10–22%, while southern China had a weak increase in GPP by only 0–6% over the same period of 2000–2015.

5.6 | Impacts of MODIS $FPAR_{C6}$ and $FPAR_{C5}$ products in China

Remote sensing-based GPP models depend heavily on the forcing data of LAI/FPAR data. MODIS FPAR C6 and C5 products had a distinct difference in interannual changes of FPAR since 2000 (Figure 8(a)). MODIS $FPAR_{C6}$ had an upward trend ($p < 0.01$) with slope $k = 0.0022$ $year^{-1}$, which was double the increase of FPAR C5 ($k = 0.001$ $year^{-1}$; $p < 0.05$). Similarly, their spatial patterns showed a large difference. $FPAR_{C6}$ data (Figure 8(b)) had more areas of increase with k higher than 0.005 $year^{-1}$compared with $FPAR_{C5}$ data (Figure 8(c)). In contrast, $FPAR_{C5}$ data had more areas of decrease with k lower than -0.0025 $year^{-1}$ when compared to $FPAR_{C6}$ data. As a result, TEC GPP_{C5} products had a lower increasing trend compared with TEC GPP_{C6} products driven with MODSI $FPAR_{C6}$ data over the same period of 2000–2015.

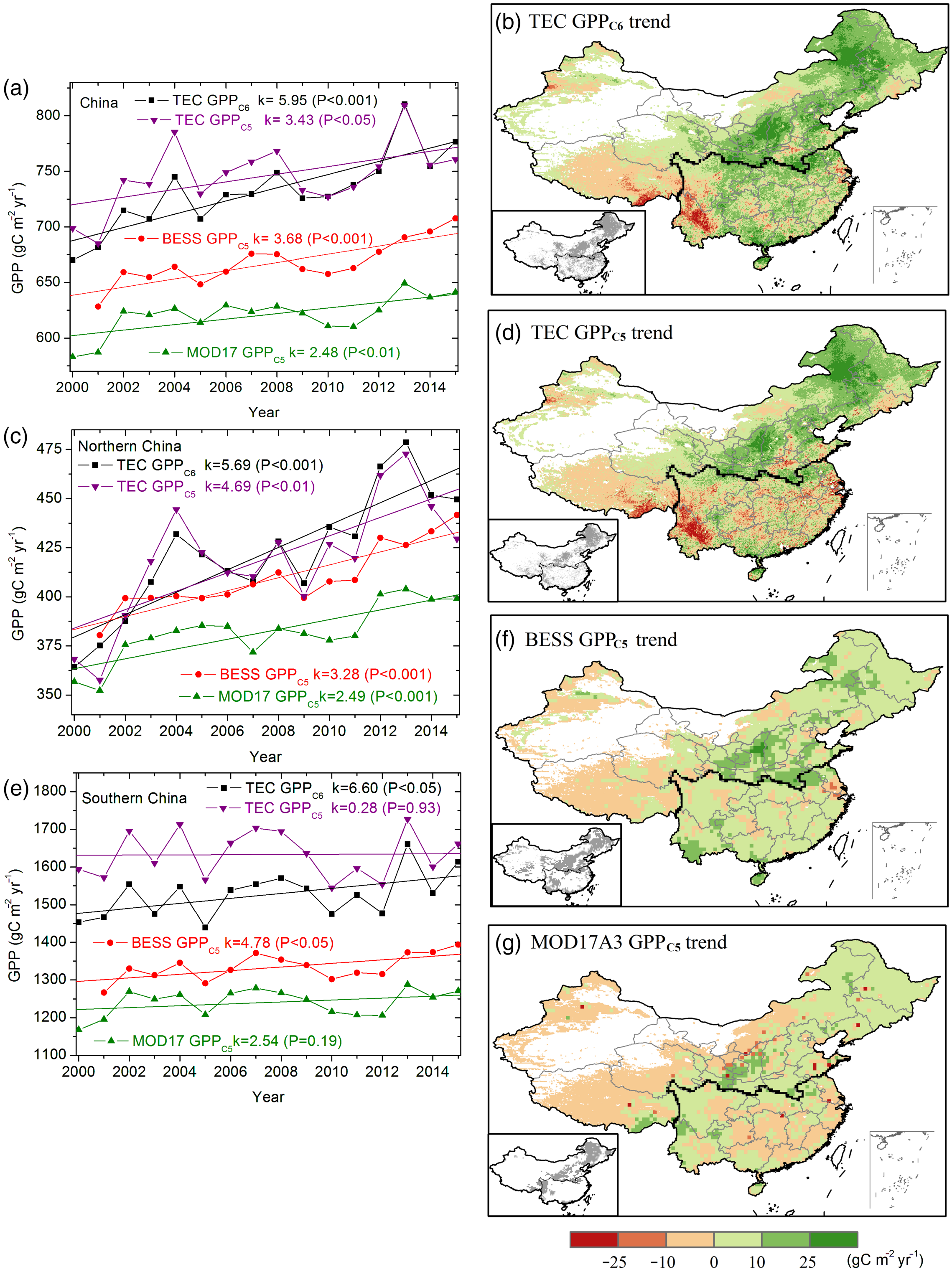

FIGURE 6 Time series of annual TEC GPP$_{C6}$, BESS GPP$_{C5}$, MOD17A3 GPP$_{C5}$, and TEC GPP$_{C5}$ in (a) China, (c) northern China, (e) southern China from 2000 to 2015 with linear trend k and significance P. spatial pattern of linear trends of annual (b) TEC GPP$_{C6}$, (d) TEC GPP$_{C5}$, (f) BESS GPP$_{C5}$, and (g) MOD17A3 GPP$_{C5}$ in China from 2000 to 2015 (Grey colour at the corner map shows trend at 0.05 significance level) [Colour figure can be viewed at wileyonlinelibrary.com]

TABLE 3 Mean annual GPP, linear trend and change rate of annual GPP over 2000–2015 for TEC GPP_{C6}, TEC GPP_{C5}, BESS GPP_{C5}, MOD17A3 GPP_{C5} products, and their ensemble mean in China, northern China, and southern China

Region	GPP	TEC GPP_{C6}	TEC GPP_{C5}	BESS GPP_{C5}	MOD17A3 GPP_{C5}	Ensemble mean
China	Mean (Pg C $year^{-1}$)	7.03	7.16	6.42	5.97	6.65
	Trend (Pg C $year^{-1}$)	0.057	0.033	0.037	0.021	0.037
	Change rate (%)	13%	7%	8%	5%	8%
Northern China	Mean (Pg C $year^{-1}$)	2.90	2.87	2.81	2.62	2.8
	Trend (Pg C $year^{-1}$)	0.039	0.032	0.022	0.017	0.028
	Change rate (%)	22%	18%	13%	10%	16%
Southern China	Mean (Pg C $year^{-1}$)	4.13	4.29	3.61	3.35	3.85
	Trend (Pg C $year^{-1}$)	0.018	0.001	0.013	0.006	0.010
	Change rate (%)	6%	0%	5%	2%	3%

TABLE 4 Correlation coefficient R and significance P of annual GPP versus PAR, T_a, P_r, and M_c over 200–2015

Region	PAR	T_a	P_r	M_c
China	−0.07 ($p = 0.79$)	0.39 ($p = 0.12$)	0.25 ($p = 0.35$)	0.62 ($p < 0.01$)
Northern China	−0.3 ($p = 0.25$)	0.06 ($p = 0.79$)	0.55 ($p < 0.05$)	0.78 ($p < 0.001$)
Southern China	0.41 ($p = 0.11$)	0.55($p < 0.05$)	0.03 ($p = 0.88$)	0.44 ($p = 0.08$)

6 | DISCUSSION

Quantifying interannual variations of GPP is key to understanding climate and vegetation dynamics. However, based on studies applying a single GPP-model, one sees large uncertainties in the interannual variations of terrestrial GPP—including the magnitude and even direction of long-term trend in China based on the application of a single model (Li *et al.,* 2013; Liu *et al.,* 2013; Wang *et al.,* 2017, 2017; Yao *et al.,* 2018).Our multi-model analysis from three GPP models found that annual GPP increased ($p < 0.05$) in China, majorly in the northern China region from 2000 to 2015, which means a wide extent of greening occurred in China. It agreed with global greening detected for the period of 1982–2014 by using satellite vegetation data and ecosystem models (Nemani *et al.,* 2003; Piao *et al.,* 2006; Zhu *et al.,* 2016, 2016). Zhu et al. (2016, 2016) reported that over 25% to 50% of global vegetated regions have a persistent and wide spread greening trend with an increasing LAI, while less than 4% of the global vegetated regions are "browning" with a decreasing LAI.

The rapid increase of GPP in China from 2000 to 2015 could be attributed to coupled effects of favourite climate, CO_2 fertilization effect, nitrogen deposition, fertilizer application, and afforestation project (Tian *et al.,* 2011; Lu *et al.,* 2012; Yuan *et al.,* 2014, 2014; Ouyang *et al.,* 2016; Fernández-Martínez *et al.,* 2017). In this study, correlation analysis shows that climate favoured the GPP increase and plant growth in China and northern China over 2000–2015, while climate inhibited GPP increase in southern China. It arose from climate-affected GPP in northern China and southern China responding to different mechanisms. For northern China, where precipitation played the dominant role in plant growth. The wet and warm climate has benefited GPP increases since 2000. For southern China, where plant was mainly stressed by radiation and heat resources not by precipitation, decreases in solar radiation played a negative impact on plant growth in southern China over 2000–2015.

Drought, as an important meteorological event, often inhibits plant growth in China. Drought monitoring for China shows an extreme drought event happened in 2000–2001 in the context of conditions during the period of 1982–2011 (Zhu *et al.,* 2016, 2016). After 2000, a wetting trend ($p < 0.01$) was obtained across China as a whole and especially in northern China. A drying trend was found for southern China until 2011 (Yan et al., 2016, 2016), which supports our results that climate change had favoured the overall increase of GPP and plant growth in China and northern China except southern China since 2000. Note that annual P_r decreased from 2000 to 2011 in southern China and then increased after 2011 (Figure 7).

Meteorological factors alone do not reconcile the negative impact of climate (Figure 7(k)) and the increases in GPP (Figure 6(e)) in southern China from 2000 to 2015. CO_2 fertilization effect has been implicated in increased vegetation greenness and land CO_2 sink (Cao *et al.,* 2002; Los, 2013; Schimel *et al.,* 2015; Fernández-Martínez *et al.,* 2017). Atmospheric CO_2 increase and climate variation contributed

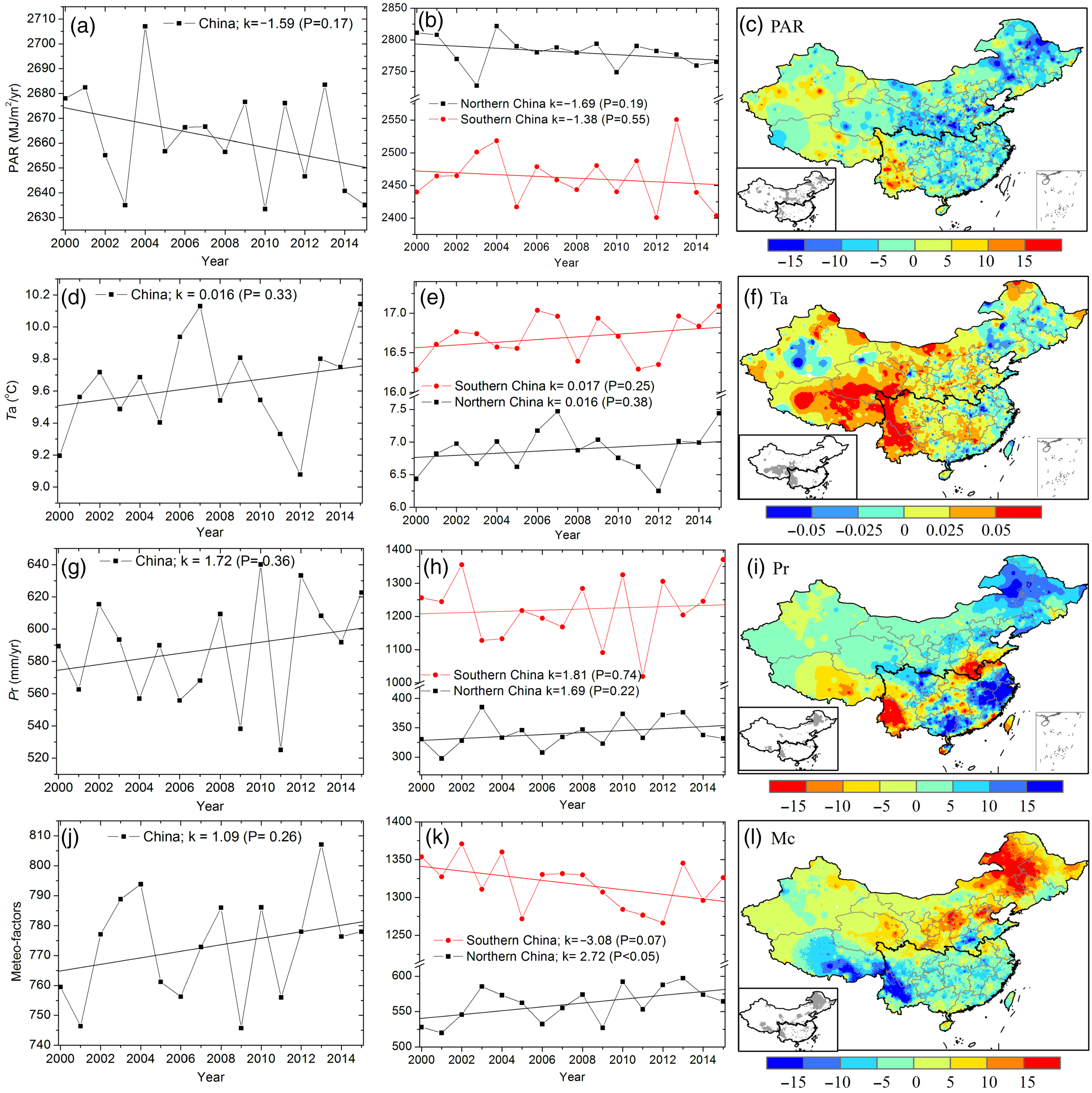

FIGURE 7 Time series of annual (a, b) PAR, (d, e) T_a, (g, h) P_r, and (j, k) Meteo-factors (M_c) in (left column) China, (middle column) northern and southern China from 2000 to 2015, and (right column) spatial patterns of their linear trends (Grey colour at the corner map show trend at 0.05 significance level) [Colour figure can be viewed at wileyonlinelibrary.com]

73% of increases of global terrestrial carbon uptake from the 1980s to the 1990s (Cao *et al.*, 2002). Los (2013) found that 40 and 40% of observed global uptrend in vegetation greenness can be explained from climate and CO_2 fertilization respectively for 1982–2006. Mao *et al*. (2016) even attributed the observed greening in the Northern Hemisphere to human-caused global change, that is, greenhouse gases. Schimel *et al*. (2015) suggested that up to 60% of the current terrestrial sink derives from CO_2 fertilization.

CO_2 fertilization not only increases plant photosynthetic rates but also alleviates the risk of drought by decreasing stomatal conductance and increasing water use efficiency (Jarvis *et al.*, 1999; Schimel *et al.*, 2015). Increasing CO_2 concentration and atmospheric humidity also alleviate forest mortality risk (Liu *et al.*, 2017). Thus, it is our assessment that CO_2 fertilization caused the weak increase in GPP by offsetting the negative impacts of climate in southern China over 2000–2015.

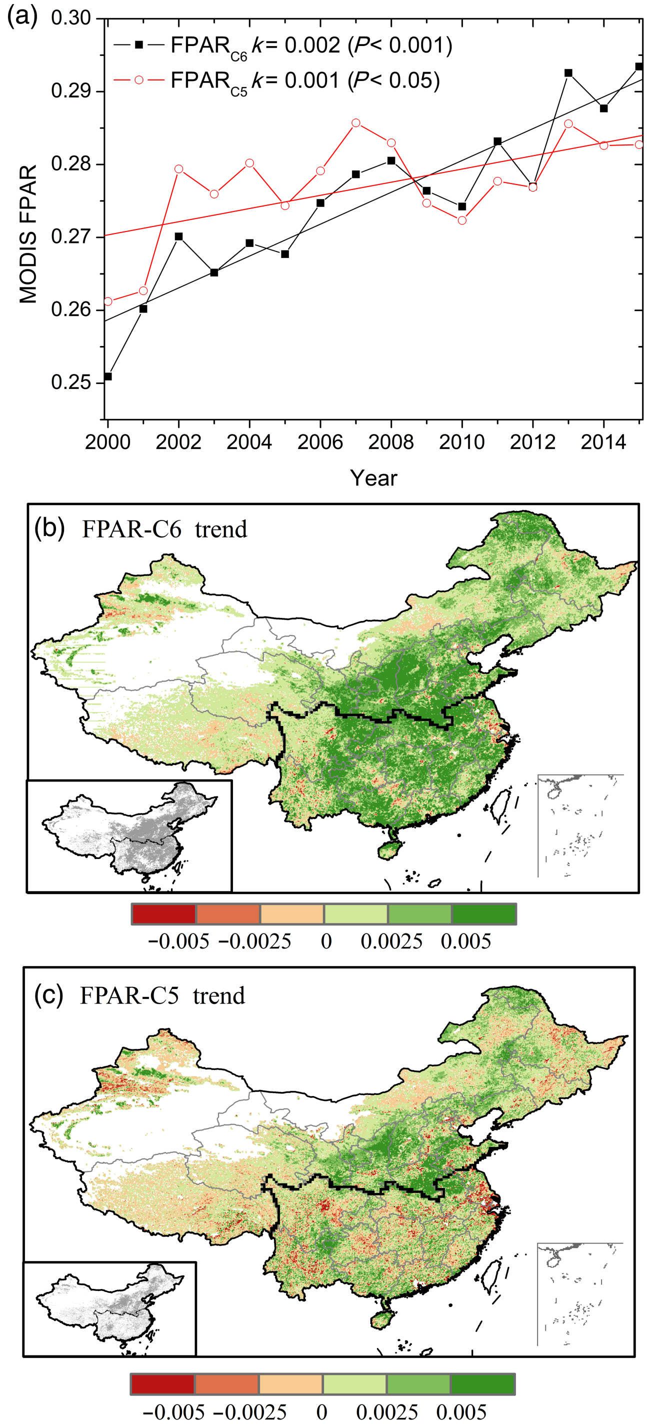

FIGURE 8 (a) Interannual variations of MODIS FPAR C6 and C5 products and spatial pattern of linear trends for annual (b) FPAR$_{C6}$ and (c) FPAR$_{C5}$ products from 2000 to 2015. The small grey map in the left corner of the figures shows trends at 0.05 significance level. The black line shows the boundary between northern China and southern China [Colour figure can be viewed at wileyonlinelibrary.com]

Meanwhile, afforestation projects as well as "Grain for Green" projects have been launched to protect and restore natural ecosystems in China. These national conservation policies lead to improvements in ecosystem services including carbon sequestration, soil retention, etc. (Yuan et al., 2014, 2014; Ouyang *et al.,* 2016). Total area of afforestation by manual planting and airplane planting increased from 2000 to 2015. The National Forestry Survey of China found the forest coverage rate (including planting forest and natural forest) increased from 18.21% for 1999–2003 to 21.63% for 2009–2013 with a net increase of 3.42%.

Studies have been applied to attribute patterns of GPP globally and regionally (Cao *et al.,* 2002; Los, 2013; Mao *et al.,* 2016; Zhu *et al.,* 2016, 2016), and accurate estimates of GPP are essential prerequisites. The TEC GPP model, as a remote sensing-based LUE model, can simulate GPP seasonality compared with flux tower-observed GPP worldwide including China (Yan *et al.,* 2015; this study), which enabled its further applications in research of interannual changes of GPP.

Evaluation of three GPP models against observed GPP at flux towers shows that MOD17 GPP products had a poor statistics and underestimated GPP with a large bias of −24.8 gC m^{-2} year^{-1}. Similarly, previous studies (Zhang *et al.,* 2008; Wang *et al.,* 2013) reported that MOD17 GPP products underestimate GPP due to the use of a low parameter value for the maximum light-use efficiency in the MOD17 algorithm. BESS and TEC GPP products had better performance statistics than MOD17 GPP products. They had an overall good performance in representing seasonal changes of plant photosynthesis. However, systematic biases still existed among these GPP estimations, consequences of using different meteorological data, MODIS FPAR and LAI data, and different GPP model structure and parameterization (Cramer *et al.,* 1999; McCallum *et al.,* 2009; Wang *et al.,* 2013).

As most LUE GPP models heavily depend on satellite derived-FPAR, we initially investigated the impact of different versions of MODIS FPAR products on GPP estimates and found that FPAR$_{C5}$ underestimated the trend by 59% compared with FPAR$_{C6}$ uptrend, resulting in an underestimated trend of TEC GPP$_{C5}$ approximating 58% of TEC GPP$_{C6}$ since 2000 in China. Similarly, Ito and Sasai (2006) reported that up to 50% difference in linear trends of interannual variability for GPP existed between driving climate datasets and GPP models. It is our assessment that the multi-model analysis can reduce uncertainties in GPP model structure and driving meteorological data.

There are uncertainties in evaluating 0.08° gridded TEC GPP data using flux tower data because the footprint of flux tower is only about 100–1,000 m. In China, flux towers are often selected for sites representing a typical regional climate and ecosystem, which allows evaluation of gridded GPP products from flux tower data. As soil data has a resolution of 5 arc-minute (i.e., 0.083°) and only 2000 stations are currently available across China, we interpolated them to a 0.08° spatial scale to drive the TEC model and further evaluated TEC GPP products by using flux tower data. The evaluation shows that TEC GPP products were capable of simulating GPP seasonal changes.

7 | CONCLUSIONS

A multi-model analysis was applied to investigate climate impacts on GPP changes in contrasting dry and wet climate zones, that is, northern China and southern China for 2000–2015. Northern China had an upward trend in annual GPP with an increasing amplitude of 2.8 times the GPP increasing trend found in southern China. For this reason, the change in northern China dominated the GPP uptrend seen for China. The upward trends of annual GPP in northern and southern China were the consequences of different mechanisms, in which climate change affected plant GPP in dry versus wet climate zones. The strong upward trend of GPP in northern China was due to more P_r in concert with higher T_a. There P_r was the dominant meteorological driver of GPP changes. The weak uptrend of GPP in southern China resulted partially from decreasing solar radiation and solar radiation exerted a key role in GPP changes. This study highlights that climate effects on GPP were subject to different mechanisms varying by climate zones in China.

MODIS C6 and C5 FPAR products had a significant difference in the calculation of interannual changes of vegetation in China. As a result, remote sensing-based GPP models driven with MODIS $FPAR_{C5}$ products, that is, TEC, BESS, and MOD17 GPP_{C5} products, gave a lower increasing trend of annual GPP in China.

Evaluation against observed GPP at nine ChinaFLUX sites across China shows that TEC GPP model simulated seasonal changes of GPP with overall statistics comparable to other model statistics. Driven with the same C5 version of MODIS FPAR/LAI products, TEC, BESS and MOD17 GPP_{C5} products all gave a comparable increase of annual GPP for the interval of 2000–2015. This study highlights that a multi-model analysis is essential in research of climate impacts on vegetation GPP with reduced uncertainties from model and driving data.

ACKNOWLEDGEMENTS

We would like to thank the Chinese Terrestrial Ecosystem Flux Observational Network (ChinaFLUX) for providing their data (http://www.chinaflux.org/), the National Meteorological Information Center (NMIC) of China for supplying meteorological data, the National Bureau of Statistics of China for sharing forest resource data (http://www.stats.gov.cn/), Chinese Ministry of Forestry for sharing forest area data, the Resource and Environment Data Center of Chinese Academy of Sciences for supplying Land cover data of China in 2000 (http://www.resdc.cn/data.aspx?DATAID=97), the Land Processes Distributed Active Archive Center (LP DAAC) managed by United States Geological Survey (USGS) for supplying MODIS data (https://lpdaac.usgs.gov/), the Numerical Terradynamic Simulation Group (NTSG) at University of Montana for supplying MOD17 GPP products (http://www.ntsg.umt.edu/), the Environmental Ecology Lab at Seoul National University for providing Breathing Earth System Simulator (BESS) GPP products, and the Oak Ridge National Laboratory Distributed Active Archive Center (ORNL DAAC) for providing global soil data (https://daac.ornl.gov). This work was supported by National Key Research and Development Program of China (2017YFC0503803), National Natural Science Foundation of China (41571327, 31700421), and National Aeronautics and Space Administration (NASA) grants to H.H. Shugart: 10-CARBON10-0068, and Climate Change/09-IDS09-116. We also thank the reviewers for their constructive remarks and suggestions.

ORCID

Hao Yan https://orcid.org/0000-0002-5287-3298

REFERENCES

Allen, R.G., Pereira, L.S., Raes, D. and Smith, M. (1998) *Crop Vapotranspiration: Guidelines for Computing Crop Water Requirements*, edn edition. Rome: Food and Agriculture Organization of the United Nations.

Baldocchi, D. (1994) A comparative-study of mass and energy-exchange rates over a closed C3 (wheat) and an open C4 (corn) crop CO2 exchange and water-use efficiency. *Agricultural and Forest Meteorology*, 67, 291–321.

Baldocchi, D., Falge, E., Gu, L.H., Olson, R., Hollinger, D., Running, S., Anthoni, P., Bernhofer, C., Davis, K., Evans, R., Fuentes, J., Goldstein, A., Katul, G., Law, B., Lee, X., Malhi, Y., Meyers, T., Munger, W., Oechel, W., Paw, U.K.T., Pilegaard, K., Schmid, H.P., Valentini, R., Verma, S., Vesala, T., Wilson, K. and Wofsy, S. (2001) FLUXNET: a new tool to study the temporal and spatial variability of ecosystem-scale carbon dioxide, water vapor, and energy flux densities. *Bulletin of the American Meteorological Society*, 82, 2415–2434.

Cao, M., Prince, S. D. & Shugart, H. H. (2002) Increasing terrestrial carbon uptake from the 1980s to the 1990s with changes in climate and atmospheric CO2. *Global Biogeochemical Cycles*, 16, 1069, doi: https://doi.org/10.1029/2001GB001553, 17-1, 17-11.

Cao, M., Prince, S.D., Tao, B., Small, J. and Li, K. (2005) Regional pattern and interannual variations in global terrestrial carbon uptake in response to changes in climate and atmospheric CO2. *Tellus B*, 57, 210–217.

Chinese Ministry of Forestry. (2004) *Forest Resource Statistics of China (1999–2003)*. Beijing, China: Department of Forest Resource and Management, Chinese Ministry of Forestry in Chinese.

Chinese Ministry of Forestry. (2014) *Forest Resource Statistics of China (2009–2013)*. Beijing, China: Department of Forest Resource and Management, Chinese Ministry of Forestry in Chinese.

Cramer, W., Kicklighter, D.W., Bondeau, A., Iii, B.M., Churkina, G., Nemry, B. and The Participants of the Potsdam NPP Model Intercomparison. (1999) Comparing global models of terrestrial net primary productivity (NPP): overview and key results. *Global Change Biology*, 5, 1–15.

Dlugokencky, E. and Tans, P.(2017) *Trends in Atmospheric Carbon Dioxide*. Boulder, Colorado: National Oceanic & Atmospheric Administration, Earth System Research Laboratory (NOAA/ESRL). http://www.esrl.noaa.gov/gmd/ccgg/trends/global.html, viewed 30 December 2017.

Falge, E., Baldocchi, D., Olson, R., Anthoni, P., Aubinet, M., Bernhofer, C., Burba, G., Ceulemans, R., Clement, R., Dolman, H., Granier, A., Gross, P., Grünwald, T., Hollinger, D., Jensen, N.O., Katul, G., Keronen, P., Kowalski, A., Lai, C.T., Law, B.E., Meyers, T., Moncrieff, J., Moors, E., Munger, J.W., Pilegaard, K., Rannik, Ü., Rebmann, C., Suyker, A., Tenhunen, J., Tu, K., Verma, S., Vesala, T., Wilson, K. and Wofsy, S. (2001) Gap filling strategies for defensible annual sums of net ecosystem exchange. *Agricultural and Forest Meteorology*, 107, 43–69.

Falge, E., Baldocchi, D., Tenhunen, J., Aubinet, M., Bakwin, P., Berbigier, P., Bernhofer, C., Burba, G., Clement, R., Davis, K.J., Elbers, J.A., Goldstein, A.H., Grelle, A., Granier, A., Guðmundsson, J., Hollinger, D., Kowalski, A.S., Katul, G., Law, B.E., Malhi, Y., Meyers, T., Monson, R.K., Munger, J.W., Oechel, W., Paw U, K.T., Pilegaard, K., Rannik, Ü., Rebmann, C., Suyker, A., Valentini, R., Wilson, K. and Wofsy, S. (2002) Seasonality of ecosystem respiration and gross primary production as derived from FLUXNET measurements. *Agricultural and Forest Meteorology*, 113, 53–74.

Fang, J., Kato, T., Guo, Z., Yang, Y., Hu, H., Shen, H., Zhao, X., Kishimoto-Mo, A.W., Tang, Y. and Houghton, R.A. (2014) Evidence for environmentally enhanced forest growth. *Proceedings of the National Academy of Sciences*, 111, 9527–9532.

Fernández-Martínez, M., Vicca, S., Janssens, I.A., Ciais, P., Obersteiner, M., Bartrons, M., Sardans, J., Verger, A., Canadell, J. G., Chevallier, F., Wang, X., Bernhofer, C., Curtis, P.S., Gianelle, D., Grünwald, T., Heinesch, B., Ibrom, A., Knohl, A., Laurila, T., Law, B.E., Limousin, J.M., Longdoz, B., Loustau, D., Mammarella, I., Matteucci, G., Monson, R.K., Montagnani, L., Moors, E.J., Munger, J.W., Papale, D., Piao, S.L. and Peñuelas, J. (2017) Atmospheric deposition, CO2, and change in the land carbon sink. *Scientific Reports*, 7, 9632.

Garbulsky, M.F., Peñuelas, J., Papale, D., Ardö, J., Goulden, M.L., Kiely, G., Richardson, A.D., Rotenberg, E., Veenendaal, E.M. and Filella, I. (2010) Patterns and controls of the variability of radiation use efficiency and primary productivity across terrestrial ecosystems. *Global Ecology and Biogeography*, 19, 253–267.

Global Soil Data Task Group. (2000) *Global Gridded Surfaces of Selected Soil Characteristics (IGBP-DIS)*. Oak Ridge, TN: ORNL DAAC. https://doi.org/10.3334/ORNLDAAC/569.

Grubb, M., Sha, F., Spencer, T., Hughes, N., Zhang, Z. and Agnolucci, P. (2015) A review of Chinese CO2 emission projections to 2030: the role of economic structure and policy. *Climate Policy*, 15, S7–S39.

He, M., Ju, W., Zhou, Y., Chen, J., He, H., Wang, S., Wang, H., Guan, D., Yan, J., Li, Y., Hao, Y. and Zhao, F. (2013) Development of a two-leaf light use efficiency model for improving the calculation of terrestrial gross primary productivity. *Agricultural and Forest Meteorology*, 173, 28–39.

Huang, K., Wang, S., Zhou, L., Wang, H., Zhang, J., Yan, J., Zhao, L., Wang, Y. and Shi, P. (2014) Impacts of diffuse radiation on light use efficiency across terrestrial ecosystems based on Eddy covariance observation in China. *Plos One*, 9, e110988.

Ito, A. and Sasai, T. (2006) A comparison of simulation results from two terrestrial carbon cycle models using three climate data sets. *Tellus B*, 58, 513–522.

Jarvis, A.J., Mansfield, T.A. and Davies, W.J. (1999) Stomatal behaviour, photosynthesis and transpiration under rising CO2. *Plant, Cell & Environment*, 22, 639–648.

Jiang, C. and Ryu, Y. (2016) Multi-scale evaluation of global gross primary productivity and evapotranspiration products derived from breathing earth system simulator (BESS). *Remote Sensing of Environment*, 186, 528–547.

Landsberg, J.J. and Waring, R.H. (1997) A generalised model of forest productivity using simplified concepts of radiation-use efficiency, carbon balance and partitioning. *Forest Ecology and Management*, 95, 209–228.

Le Quéré, C., Andrew, R.M., Canadell, J.G., Sitch, S., Korsbakken, J. I., Peters, G.P., Manning, A.C., Boden, T.A., Tans, P.P., Houghton, R.A., Keeling, R.F., Alin, A., Andrews, O.D., Anthoni, P., Barbero, L., Bopp, L., Chevallier, F., Chini, L.P., Ciais, P., Currie, K., Delire, C., Doney, S.C., Friedlingstein, P., Gkritzalis, T., Harris, I., Hauck, J., Haverd, V., Hoppema, M., Goldewijk, K.K., Jain, A.K., Kato, E., Körtzinge, A., Landschützer, P., Lefèvre, N., Lenton, A., Lienert, S., Lombardozzi, D., Melton, J.R., Metzl, N., Millero, F., Monteiro, P. M.S., Munro, D.R., Nabel, J.E.M.S., Nakaoka, S., O'Brien, K., Olsen, A., Omar, A.M., Ono, T., Pierrot, D., Poulter, B., Rödenbeck, C., Salisbury, J., Schuster, U., Schwinger, J., S'ef'erian, R., Skjelvan, I., Stocker, B.D., Sutton, A.J., Takahashi, T., Tian, H., Tilbrook, B., van der Laan-Luijkx, I.T., van der Werf, G.R., Viovy, N., Walker, A.P., Wiltshire, A.J. and Zaehle, S. (2016) Global carbon budget 2016. *Earth System Science Data*, 8, 605–649.

Li, X.L., Liang, S.L., Yu, G.R., Yuan, W., Cheng, X., Xia, J., Zhao, T. B., Feng, J.M., Ma, Z.G., MA, M.G., Liu, S.M., Chen, J.Q., Shao, C.L., Li, S.G., Zhang, S.D., Zhang, Z.Q., Chen, S.P., Ohta, T., Vaelagin, A., Miyata, A., Takagi, K., Saiqusa, N. and Kato, T. (2013) Estimation of gross primary production over the terrestrial ecosystems in China. *Ecological Modelling*, 261-262, 80–92.

Liu, Y., Ju, W., He, H., Wang, S., Sun, R. and Zhang, Y. (2013) Changes of net primary productivity in China during recent 11 years detected using an ecological model driven by MODIS data. *Frontiers of Earth Science*, 7, 112–127.

Liu, J., Liu, M., Deng, X., Zhuang, D., Zhang, Z. and Luo, D. (2002) The land use and land cover change database and its relative studies in China. *Journal of Geographical Sciences*, 12, 275–282.

Liu, J., Liu, M., Zhuang, D., Zhang, Z. and Deng, X. (2003) Study on spatial pattern of land-use change in China during 1995–2000. *Science in China Series D: Earth Sciences*, 46, 373–384.

Liu, Y., Parolari, A.J., Kumar, M., Huang, C.-W., Katul, G.G. and Porporato, A. (2017) Increasing atmospheric humidity and CO2 concentration alleviate forest mortality risk. *Proceedings of the National Academy of Sciences*, 114, 9918–9923.

Los, S.O. (2013) Analysis of trends in fused AVHRR and MODIS NDVI data for 1982–2006: indication for a CO2 fertilization effect in global vegetation. *Global Biogeochemical Cycles*, 27, 318–330.

Lu, C., Tian, H., Liu, M., Ren, W., Xu, X., Chen, G. and Zhang, C. (2012) Effect of nitrogen deposition on China's terrestrial carbon uptake in the context of multifactor environmental changes. *Ecological Applications*, 22, 53–75.

Lyapustin, A., Wang, Y., Xiong, X., Meister, G., Platnick, S., Levy, R., Franz, B., Korkin, S., Hilker, T., Tucker, J., Hall, F., Sellers, P., Wu, A. and Angal, A. (2014) Scientific impact of MODIS C5 calibration degradation and C6+ improvements. *Atmospheric Measurement Techniques*, 7, 4353–4365.

Maisongrande, P., Ruimy, A., Dedieu, G. and Saugier, B. (1995) Monitoring seasonal and interannual variations of gross primary productivity, net primary productivity and net ecosystem productivity using a diagnostic model and remotely-sensed data. *Tellus B*, 47, 178–190.

Mao, J., Ribes, A., Yan, B., Shi, X., Thornton, P.E., Séférian, R., Ciais, P., Myneni, R.B., Douville, H., Piao, S., Zhu, Z., Dickinson, R.E., Dai, Y., Ricciuto, D.M., Jin, M., Hoffman, F.M., Wang, B., Huang, M. and Lian, X. (2016) Human-induced greening of the northern extratropical land surface. *Nature Climate Change*, 6, 959–963.

McCallum, I., Wagner, W., Schmullius, C., Shvidenko, A., Obersteiner, M., Fritz, S. and Nilsson, S. (2009) Satellite-based terrestrial production efficiency modeling. *Carbon Balance and Management*, 4, 8.

McCree, K.J. (1972) Test of current definitions of phtosysthetically active radiation against leaf photosysthesis data. *Agricultural Meteorology*, 10, 442–453.

Millar, R.J., Fuglestvedt, J.S., Friedlingstein, P., Rogelj, J., Grubb, M. J., Matthews, H.D., Skeie, R.B., Forster, P.M., Frame, D.J. and Allen, M.R. (2017) Emission budgets and pathways consistent with limiting warming to 1.5 °C. *Nature Geoscience*, 10, 741–747.

Monteith, J.L. (1972) Solar radiation and productivity in tropical ecosystems. *Journal of Applied Ecology*, 9, 747–766.

Myneni, R.B., Hoffman, S., Knyazikhin, Y., Privette, J.L., Glassy, J., Tian, Y., Wang, Y., Song, X., Zhang, Y., Smith, G.R., Lotsch, A., Friedl, M., Morisette, J.T., Votava, P., Nemanic, R.R. and Running, S.W. (2002) Global products of vegetation leaf area and fraction absorbed PAR from year one of MODIS data. *Remote Sensing of Environment*, 83, 214–231.

National Meteorological Information Center. (2010) *Meteorological industry standard of the People's Republic of China: Quality control of surface meteorological observational data (QX/T 118-2010)*. Beijing, China: China Meteorological Press (In Chinese).

Nemani, R.R., Keeling, C.D., Hashimoto, H., Jolly, W.M., Piper, S.C., Tucker, C.J., Myneni, R.B. and Running, S.W. (2003) Climate-driven increases in global terrestrial net primary production from 1982 to 1999. *Science*, 300, 1560–1563.

Ouyang, Z., Zheng, H., Xiao, Y., Polasky, S., Liu, J., Xu, W., Wang, Q., Zhang, L., Xiao, Y., Rao, E., Jiang, L., Lu, F., Wang, X., Yang, G., Gong, S., Wu, B., Zeng, Y., Yang. W., Daily, G. C. (2016) Improvements in ecosystem services from investments in natural capital. *Science*, 352, 1455–1459.

Pfeifer, M., Disney, M., Quaife, T. and Marchant, R. (2012) Terrestrial ecosystems from space: a review of earth observation products for macroecology applications. *Global Ecology and Biogeography*, 21, 603–624.

Piao, S., Friedlingstein, P., Ciais, P., Zhou, L. and Chen, A. (2006) Effect of climate and CO_2 changes on the greening of the northern hemisphere over the past two decades. *Geophysical Research Letters*, 33, 1–6.

Priestley, C.H. and Taylor, R.J. (1972) Assessment of surface heat-flux and evaporation using large-scale parameters. *Monthly Weather Review*, 100, 81–92.

Prince, S.D. and Goward, S.N. (1995) Global primary production: a remote sensing approach. *Journal of Biogeography*, 22, 815–835.

Raich, J.W., Rastetter, E.B., Melillo, J.M., Kicklighter, D.W., Steudler, P.A., Peterson, B.J., Grace, A.L., Moore, B., III and Vorosmarty, C.J. (1991) Potential net primary productivity in South-America - application of a global-model. *Ecological Applications*, 1, 399–429.

Ruimy, A., Kergoat, L., Bondeau, A. and The participants of the Potsdam NPP Model Intercomparison. (1999) Comparing global models of terrestrial net primary productivity (NPP): analysis of differences in light absorption and light-use efficiency. *Global Change Biology*, 5, 56–64.

Running, S.W., Nemani, R.R., Heinsch, F.A., Zhao, M.S., Reeves, M. and Hashimoto, H. (2004) A continuous satellite-derived measure of global terrestrial primary production. *Bioscience*, 54, 547–560.

Ryu, Y., Baldocchi, D.D., Kobayashi, H., Van Ingen, C., Li, J., Black, T.A., Beringer, J., van Gorsel, E., Knohl, A., Law, B.E. and Roupsard, O. (2011) Integration of MODIS land and atmosphere products with a coupled-process model to estimate gross primary productivity and evapotranspiration from 1 km to global scales. *Global Biogeochemical Cycles*, 25, Gb4017. https://doi.org/10.1029/2011gb004053.

Schimel, D., Stephens, B.B. and Fisher, J.B. (2015) Effect of increasing CO2 on the terrestrial carbon cycle. *Proceedings of the National Academy of Sciences*, 112, 436–441.

Tian, H., Melillo, J., Lu, C., Kicklighter, D., Liu, M., Ren, W., Xu, X., Chen, G., Zhang, C., Pan, S., Liu, J. and Running, S. (2011) China's terrestrial carbon balance: contributions from multiple global change factors. *Global Biogeochemical Cycles*, 25, GB1007. https://doi.org/10.1029/2010GB003838.

Verma, S.B., Dobermann, A., Cassman, K.G., Walters, D.T., Knops, J. M., Arkebauer, T.J., Suyker, A.E., Burba, G.G., Amos, B., Yang, H., Ginting, D., Hubbard, K.G., Gitelson, A.A. and Walter-Shea, E.A. (2005) Annual carbon dioxide exchange in irrigated and rainfed maize-based agroecosystems. *Agricultural and Forest Meteorology*, 131, 77–96.

Wang, J., Dong, J., Yi, Y., Lu, G., Oyler, J., Smith, W.K., Zhao, M., Liu, J. and Running, S. (2017) Decreasing net primary production due to drought and slight decreases in solar radiation in China from 2000 to 2012. *Journal of Geophysical Research: Biogeosciences*, 122(1), 261–278.

Wang, Y., Kang, M., Zhao, M., Xing, K., Wang, G. and Xue, F. (2017) The spatiotemporal variation of tree cover in the loess plateau of China after the 'grain for green' project. *Sustainability*, 9, 739.

Wang, X., Ma, M., Li, X., Song, Y., Tan, J., Huang, G., Zhang, Z., Zhao, T., Feng, J., Ma, Z., Wei, W. and Bai, Y. (2013) Validation of MODIS-GPP product at 10 flux sites in northern China. *International Journal of Remote Sensing*, 34(2), 587–599.

Wang, D., Morton, D., Masek, J., Wu, A., Nagol, J., Xiong, X., Levy, R., Vermote, E. and Wolfe, R. (2012) Impact of sensor degradation on the MODIS NDVI time series. *Remote Sensing of Environment*, 119, 55–61.

Wang, L., Zheng, Y., Yu, Q. and Wang, E. (2007) Applicability of AgriculturalProduction systems simulator (APSIM) in simulating the production and water use of wheat-maize continuous cropping system in North China plain. *Chinese Journal of Applied Ecology*, 18, 2480–2486.

Wang, Q., Zheng, H., Zhu, X. and Yu, G. (2015) Primary estimation of Chinese terrestrial carbon sequestration during 2001–2010. *Science Bulletin*, 60, 577–590.

Waring, R.H., Law, B.E., Goulden, M.L., Bassow, S.L., Mccreight, R. W., Wofsy, S.C. and Bazzaz, F.A. (1995) Scaling gross ecosystem production at Harvard Forest with remote sensing: a comparison of estimates from a constrained quantum-use efficiency model and eddy correlation. *Plant, Cell & Environment*, 18, 1201–1213.

Yan, H., Wang, S.Q., Billesbach, D., Oechel, W., Bohrer, G., Meyers, T., Martin, T.A., Matamala, R., Phillips, R.P., Rahman, F., Yu, Q. and Shugart, H.H. (2015) Improved global simulations of gross primary product based on a new definition of water stress factor and a separate treatment of C3 and C4 plants. *Ecological Modelling*, 297, 42–59.

Yan, H., Wang, S.Q., Billesbach, D., Oechel, W., Zhang, J.H., Meyers, T., Martin, T.A., Matamala, R., Baldocchi, D., Bohrer, G., Dragoni, D. and Scott, R. (2012) Global estimation of evapotranspiration using a leaf area index-based surface energy and water balance model. *Remote Sensing of Environment*, 124, 581–595.

Yan, H., Wang, S.-Q., Wang, J.-B., Lu, H.-Q., Guo, A.-H., Zhu, Z.-C., Myneni, R.B. and Shugart, H.H. (2016) Assessing spatiotemporal variation of drought in China and its impact on agriculture during 1982–2011 by using PDSI indices and agriculture drought survey data. *Journal of Geophysical Research: Atmospheres*, 121, 2283–2298.

Yang, W.Z., Huang, D., Tan, B., Stroeve, J.C., Shabanov, N.V., Knyazikhin, Y. and Myneni, R.B. (2006) Analysis of leaf area index and fraction of PAR absorbed by vegetation products from the terra MODIS sensor: 2000-2005. *IEEE Transactions on Geoscience and Remote Sensing*, 44, 1829–1842.

Yao, Y., Wang, X., Li, Y., Wang, T., Shen, M., Du, M., H He, Y Li, W Luo, M Ma, Y Ma, Y Tang, H Wang, X Zhang, Y Zhang, L Zhao, G Zhou Piao, S. (2018) Spatiotemporal pattern of gross primary productivity and its covariation with climate in China over the last thirty years. *Global Change Biology*, 24, 184–196.

Yu, G.-R., Zhu, X.-J., Fu, Y.-L., He, H.-L., Wang, Q.-F., Wen, X.-F., Li, X.R., Zhang, L.M., Zhang, L., Su, W., Li, S.G., Sun, X.M., Zhang, Y.P., Zhang, J.H., Yan, J.H., Wang, H.M., Zhou, G.S., Jia, B.R., Xiang, W.H., Li, Y.N., Zhao, L., Wang, Y.F., Shi, P.L., Chen, S.P., Xin, X.P., Zhao, F.H., Wang, Y.Y. and Tong, C.-L. (2013) Spatial patterns and climate drivers of carbon fluxes in terrestrial ecosystems of China. *Global Change Biology*, 19, 798–810.

Yuan, W., Li, X., Liang, S., Cui, X., Dong, W., Liu, S., Xia, J., Chen, Y., Liu, D. and Zhu, W. (2014) Characterization of locations and extents of afforestation from the grain for green project in China. *Remote Sensing Letters*, 5, 221–229.

Yuan, W., Liu, D., Dong, W., Liu, S., Zhou, G., Yu, G., Zhao, T., Feng, J., Ma, Z., Chen, J., Chen, Y., Chen, S., Han, S., Huang, J., Li, L., Liu, H., Liu, S., Ma, M., Wang, Y., Xia, J., Xu, W., Zhang, Q., Zhao, X. and Zhao, L. (2014) Multiyear precipitation reduction strongly decreases carbon uptake over northern China. *Journal of Geophysical Research: Biogeosciences*, 119, 881–896. https://doi.org/10.1002/2014JG002608.

Zhang, Y., Song, C., Band, L.E., Sun, G. and Li, J. (2017) Reanalysis of global terrestrial vegetation trends from MODIS products: Browning or greening? *Remote Sensing of Environment*, 191, 145–155.

Zhang, L., Xiao, J., Li, J., Wang, K., Lei, L. and Guo, H. (2012) The 2010 spring drought reduced primary productivity in southwestern China. *Environmental Research Letters*, 7(4), 045706. https://doi.org/10.1088/1748-9326/7/4/045706.

Zhang, Y., Yu, Q., Jiang, J.I.E. and Tang, Y. (2008) Calibration of Terra/MODIS gross primary production over an irrigated cropland on the North China plain and an alpine meadow on the Tibetan plateau. *Global Change Biology*, 14, 757–767.

Zhang, T., Zhang, Y., Xu, M., Zhu, J., Chen, N., Jiang, Y., Huang, K., Zu, J., Liu, Y. and Yu, G. (2018) Water availability is more important than temperature in driving the carbon fluxes of an alpine meadow on the Tibetan plateau. *Agricultural and Forest Meteorology*, 256-257, 22–31. https://doi.org/10.1016/j.agrformet.2018.02.027.

Zhao, M. and Running, S.W. (2010) Drought-induced reduction in global terrestrial net primary production from 2000 through 2009. *Science*, 329, 940–943.

Zhu, H., Lin, A., Wang, L., Xia, Y. and Zou, L. (2016) Evaluation of MODIS Gross primary production across multiple biomes in China using Eddy covariance flux data. *Remote Sensing*, 8, 395. https://doi.org/10.3390/rs8050395.

Zhu, Z., Piao, S., Myneni, R.B., Huang, M., Zeng, Z., Canadell, J.G., Ciais, P., Sitch, S., Friedlingstein, P., Arneth, A., Cao, C., Cheng, L., Kato, E., Koven, C., Li, Y., Lian, X., Liu, Y., Liu, R., Mao, J., Pan, Y., Peng, S., Peñuelas, J., Poulter, B., Pugh, T.A.M., Stocker, B.D., Viovy, N., Wang, X., Wang, Y., Xiao, Z., Yang, H., Zaehle, S. and Zeng, N. (2016) Greening of the earth and its drivers. *Nature Climate Change*, 6, 791–795.

How to cite this article: Yan H, Wang S, Wang J, *et al.* Multi-model analysis of climate impacts on plant photosynthesis in China during 2000–2015. *Int J Climatol*. 2019;39:5539–5555. https://doi.org/10.1002/joc.6170